# X-Ray Studies on Substructures in Single Crystals of Tin. (II)

## Substructures of Tin as Related to its Purity

Masashige KOYAMA*

(H. Takaki Laboratory)

*Received July 3, 1958*

The relation between the substructures mentioned in Part I and the purity was investigated, by the X-ray diffraction microscopy, with tin which had been zone-refined by using the reciprocating process.

In single crystals which were grown by using the zone-refined tin at 0.8 mm/min and in the [110] direction, no linear substructures appeared and the reticulate substructures of irregular shape were fewer in number too, as compared with the specimen grown from the less pure tin.

As to the perfection of crystals, no difference was observed between two specimens grown at 0.05 and 0.8 mm/min respectively by using the zone-refined tin. Namely, the speed of growth, at least within a certain limit, seems to have no influence upon the perfection of crystals. Therefore, the necessary thing is high purity.

### I. INTRODUCTION

In Part I, the relations of the substructures, which were observed in the single crystals of tin grown from the melt, with the temperature gradient, speed of growth and purity, were examined by the X-ray diffraction microscopy. As the three kinds of tin so far used, however, were prepared by different manufactures, a detailed investigation on the relation between the purity and the substructures was impossible.

In this study, this relation was examined by using the zone-refined tin with the same method as used in the previous study.

### II. EXPERIMENTAL PROCEDURES

#### 1. Zone-Refining

Although there are several methods in the zone-refining[1][2], the reciprocating process[3] was adopted in this study. Fig. 1 shows a part of the equiment. Three electric furnaces H for the zone-refining could be moved along a Terex glass tube G. In the present research, only the left two were used. The temperatures of the furnaces were controlled independently. In order to reduce the width of molten zone and to make the temperature gradient steeper, the both sides of each furnace were equiped with the coolers which moved together with the furnaces. After the raw tin was put in a glass tube of an inner diameter of

* 小 山 昌 重

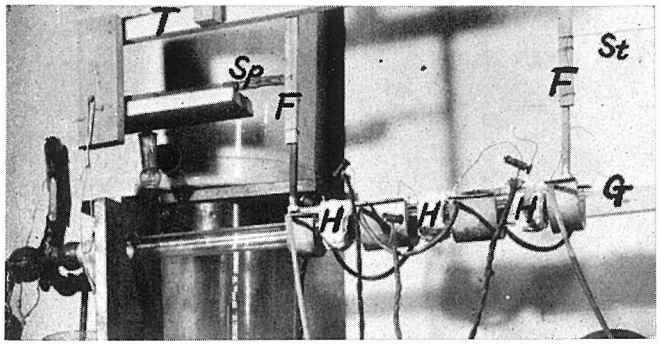


Fig. 1. A part of the equipment used for zone-refining.

1 cm, the both ends of this tube were bent upward a little to prevent overflow of the molten tin. The tube was placed in G so that the left end of the raw tin came to the left end of the left-hand furnace. G was evacuated with the vacuum pump ($10^{-3}$~$10^{-4}$ mm Hg). The electric furnaces were connected with the frame F, the upper part of which could be moved on the track T. The left end of the frame was pulled by the spring Sp, and its right end was pulled by the string St at a constant speed. When the left-hand furnace moved to the place where the central one had been situated, it returned to the original place automatically by Sp. The interval between the right end of the left-hand furnace and the left end of the central one was 8 cm.

## 2. Method of Analysis

The zone-refined tin was analyzed by using a spectroscope of the Litro type. As the standard specimen of tin was not available, the perfect quantitative analysis could not be made. One of the electrodes was the section of the specime and the other was the carbon rod. A filter consisting of three subfilters having different penetrating rates (26, 100, and 4%) was used. The wave lengths of the spectra measured are indicated at the left end of Fig. 2.

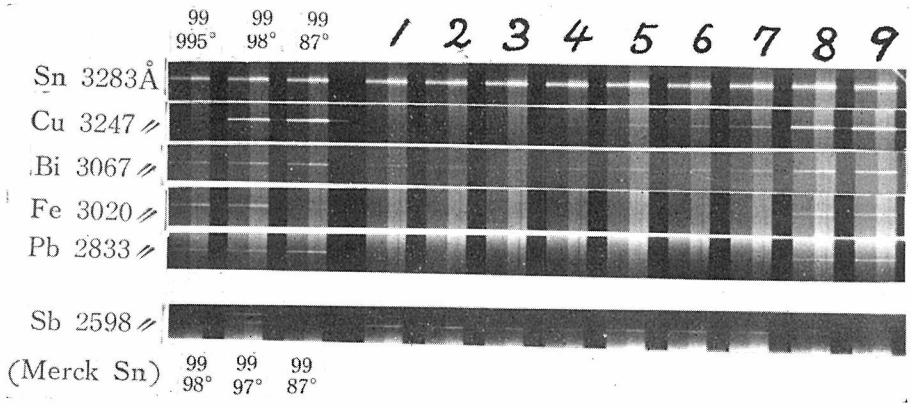


Fig. 2. Spectrographic pattern of the specimen zone-refined by using 99.98% pure tin at 0.5 mm/min.

The result of the analysis is represented as follows :

$$\Delta S = \log (d_{Sn}/d_I)$$

where $d_{Sn}$ and $d_I$ indicate respectively the deflections of the galvanometer which are in inverse proportion to the intensities of the spectrum of tin and the spectrum of one of the impurities. The values of $\Delta S$ were plotted on the vertical axis and the positions of nine sections obtained by dividing the refined specimen into ten equal parts were on the horizontal axis.

### 3. Result of Analysis

The refining conditions of tin used for the X-ray analysis are given in Table 1 : purity of the raw tin used for refining ; width of molten zone ; length of specimen ; moving speed of electric furnace ; number of zone pass.

Table 1.

| Purity | Zone | Length | Speed | Pass |
|---|---|---|---|---|
| 99.98% | 5 cm | 22 cm | 0.5 mm/min | 20 times |
| 99.99% | 5 cm | 25 cm | 0.6 mm/min | 20 times |

The result of zone-refining of 99.98% pure tin is shown in Fig. 2. The image of each spectrum consists of three lines which passed through the sub-filters of different penetrating rates (26, 100 and 4%).

Copper, lead and iron were always segregated at the part of the specimen which froze last. Bismuth, however, could not be refined sufficiently. Judging from the equilibrium diagram of the tin-antimony system, antimony is considered to concentrate at the portion which froze first. In case of 99.98% pure tin in which antimony was small in amount, however, antimony concentrated at the part of the specimen which froze later (photograph is not shown). On the other hand, Merck tin (99.97%), in which antimony was relatively large in amount, was zone-refined under the same condition as that for 99.98% pure tin. As seen at the bottom of Fig. 2, antimony concentrated fairly rich at the part of the specimen which froze first.

Figs. 3 and 4* show the results of analysis of two kinds of specimens indicated in Table 1.

In either case, the third and fourth blocks at the left of the specimen were highest in purity. Therefore, these parts were used as the materials of the single crystals for X-ray analysis.

### 4. X-Ray Diffraction Microscopy

The X-ray unit and the condition and method of photography were similar to those reported in Part I except that the specimen-to-plate distance was 400 mm.

* $\Delta S$ of impurities of the raw tin was indicated at the left end of each figure. The fog of the plate was deducted.
For convenience, $\Delta s$ in Figs. 3 and 4 is indicated by the values of $d_{Sn}/d_I$ instead of $\log (d_{Sn}/d_I)$.

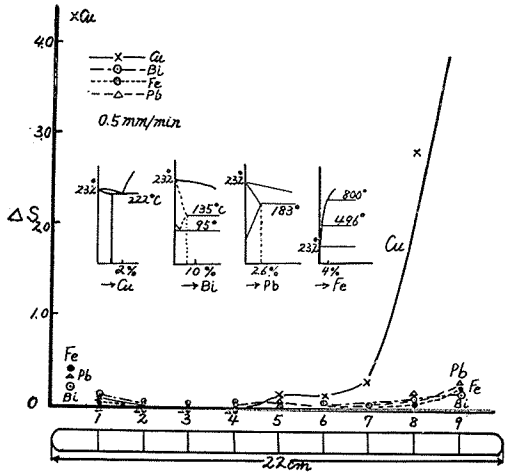


Fig. 3. Result of the spectrographic analysis of the specimen zone-refined by using 99.98% pure tin at 0.5 mm/min.

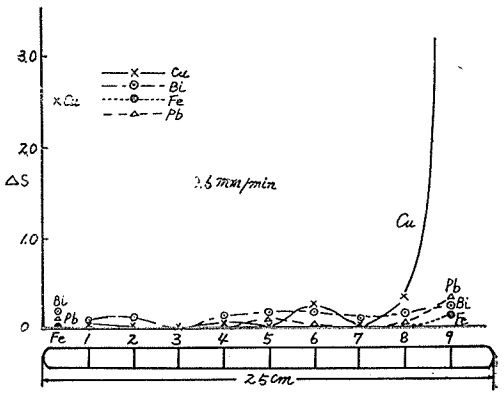


Fig. 4. Result of the spectrographic analysis of the specimen zone-refined by using 99.99% pur tin at 0.6 mm/min.

## III. EXPERIMENTAL RESULTS

### 1. 99.98% Pure Tin and Temperature Gradient of 45°/cm

(1) **Tin before refined.** (i) Side surface of specimen. The Berg puttern of the side surface (001) of the single crystal* which was grown in the [110] direction at 0.8 mm/min, is shown in Fig. 5.**

It seems that the two subboundarirs '*a*' and '*b*' running in the center of the photograph developed from the seed. Besides, the linear subboundaries which develop newly in the direction of crystal growth are observed. The number of these subboundaries increases with the increase of the distance from the seed. Further, the block-like substructures of irregular shape are observed. Their dimensions are 0.1~2 mm and the differences in the crystallographic orientation are 2~5 min of arc. Fig. 6 shows the enlargement of a part of the lower photograph in Fig. 5 ($\alpha$ is 21.6 degrees). The width of the black line indicating the orientation difference of the subboundary '*a*' is narrow at the place where it crosses the substructures of irregular shape (indicated by arrows).

The linear subboundary running in the direction of growth seems to develop from one of the subboundaries of irregular shape. This example is shown by

* Every single crystal which will be examined hereinafter, is grown in the [110] direction by using an elliptic cross section glass tube. In the X-ray analysis, the side surface (001) vertical to the minor axis of the elliptic cross section will be used as the specimen face.

** In order to examine the broad area of the surface the specimen was moved two or three times and the reflected images taken by changing $\alpha$ each time were jointed together. (The direction of growth is from right to left; upper photograph shows the result of the place near the seed.) The photograph is obscure because the images, which are different in intensity, are jointed together.

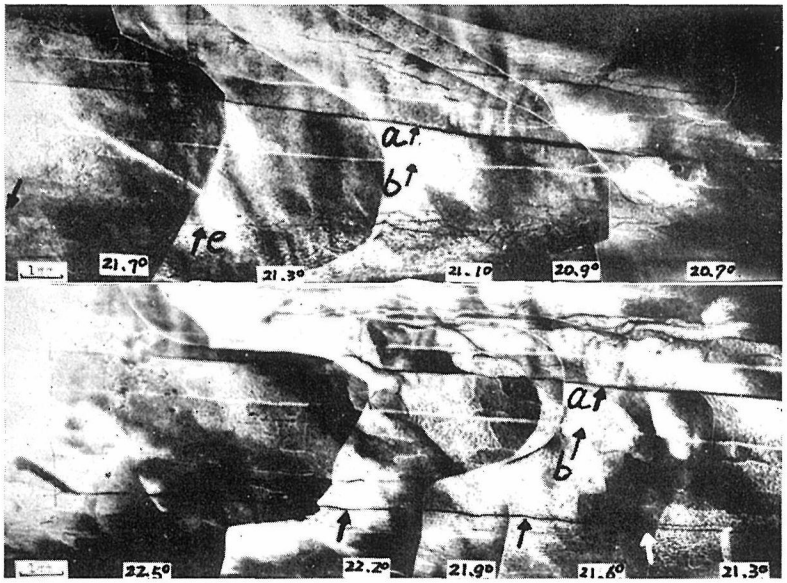


Fig. 5. X-ray micrographs of the side surface (001) of the specimen (99.98% pure tin) grown at 0.8 mm/min and 45°/cm. A series of reflected images taken by changing $\alpha$, were joined together. Fe K$\alpha$, specimen face : (001), reflecting plane : (332).

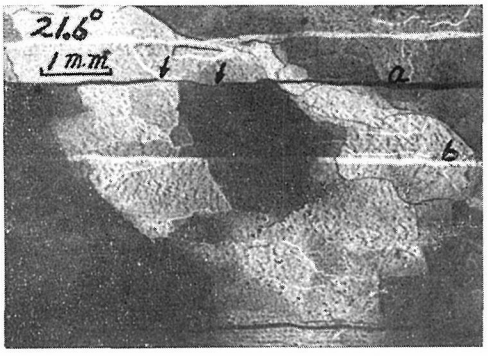


Fig. 6. Enlarged X-ray micrograph of a part of the lower photograph in Fig 5.

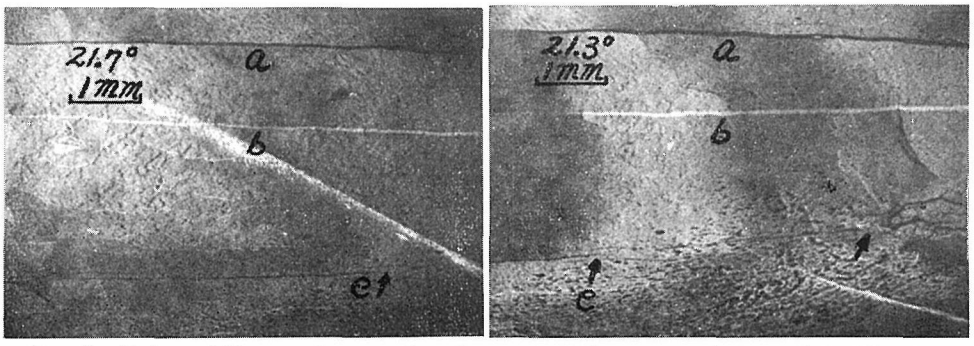


Fig. 7. Enlarged X-ray micrographs of a part of the upper photograph in Fig. 5.

the arrows in Figs. 5 and 7.* (The latter is the enlargement of a part of the upper photographs in Fig. 5.)

Fig. 8 shows the Berg pattern of the cross section (110) of the specimen shown in Fig. 5. In this case, the specimen was cut at the place near the part which froze last. (The image of the broad black line at the right upper part is a scratch.)

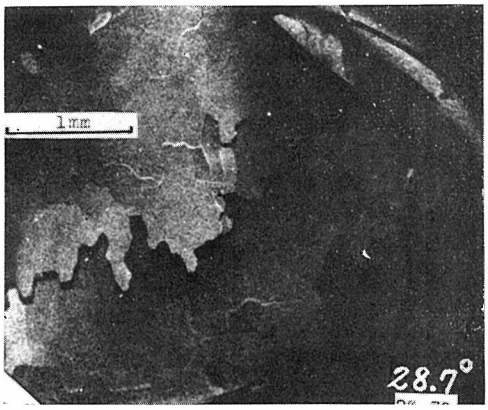


Fig. 8. X-ray micrograph of the cross section (110) of the specimen in Fig. 5. Cu K$\alpha$, specimen face : (110), reflecting plane : (620).

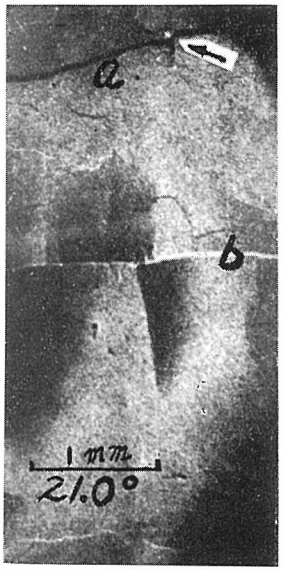


Fig. 9. X-ray micrograph of the inner part of the specimen in Fig. 5. Fe K$\alpha$, specimen face : (001), reflecting plane: (211).

(ii) Inside of specimen. After the specimen of Fig. 5 was electropolished until its width becomes about a half of the original one, the inside of the specimen was examined. In the electropolished specimen, too, the subboundaries ('*a*' and '*b*') could be observed almost at the same place as that in Fig. 5. The subboundaries of irregular shape were also observed in the same specimen. (Photograph is not shown.) Fig. 9 shows the Berg pattern of the (211) plane. A kind of fault can be observed at the point on the subboundary '*a*' (indicated by an arrow in the figure).

(2) **Zone-refined tin.** The third and the fourth blocks of the left of the zone-refined tin shown in Fig. 4 were used as the material of the single crystal. The specimen was prepared from the same seed as that in Fig. 5.** In this case, the (001) and (332) planes were used as the specimen face and the reflecting plane respectively. The Berg pattern is shown in Fig. 10.*** The

* The reflected image running obliquely in the photograph is that of another plane.

** This seed was prepared by using the zone-refined tin from the same seed as that in Fig. 5. The speed of growth is 0.8 mm/min and the direction of growth is [110].

*** See the foot-note (**) on page 65.

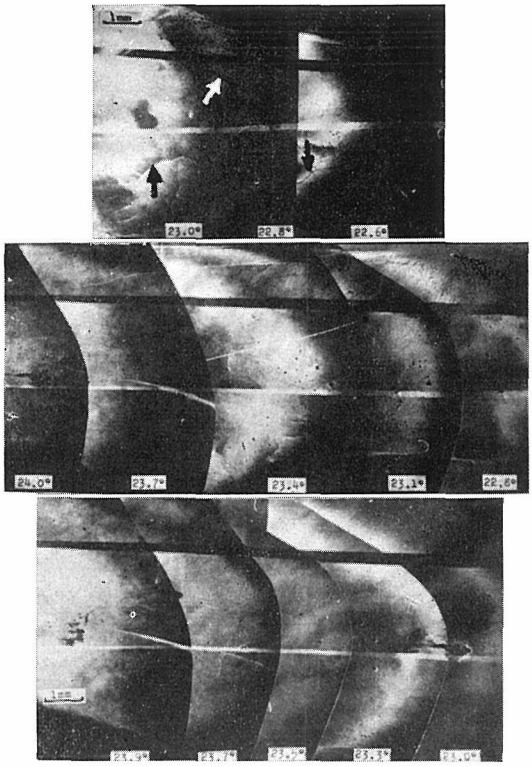

Fig. 10. X-ray micrographs of the side surface (001) of the specimen (zone-refined tin) grown at 0.8 mm/min and 45°/cm. A series of reflected images taken by changing $\alpha$, were jointed together. Fe K$\alpha$, specimen face : (001), reflecting plane : (332).

substructures of irregular shape are obscurely observed, but the linear subboundary is not. The orientation differences of these subboundaries could not be determined because of the low sensitivity of the equipment. The substructures of irregular shape appear especially at the part where both the width and the thickness of the specimen increase gradually (arrows in the top photograph.) These substructures are fewer in number, however, as compared with those in the specimen of less pure tin.

### 2. 99.99% Pure Tin and Temperature Gradient of 13°/cm

The influences of the purity, temperature gradient and speed of growth on the substructures, were examined again.

(1) **Tin before zone-refined.** In the specimen grown in the [110] direction at 0.8 mm/min, several linear subboundaries are observed at the place near the part which froze last. Fig. 11 shows the Berg pattern of the place mentioned above. Besides the subboundaries 's' developing from the seed, the linear subboundary of black or white line develops newly from the reticulate subboundary of black or white one respectively as indicated by arrows.

(2) **Zone-refined tin.** The second, third and fourth blocks of the left of the

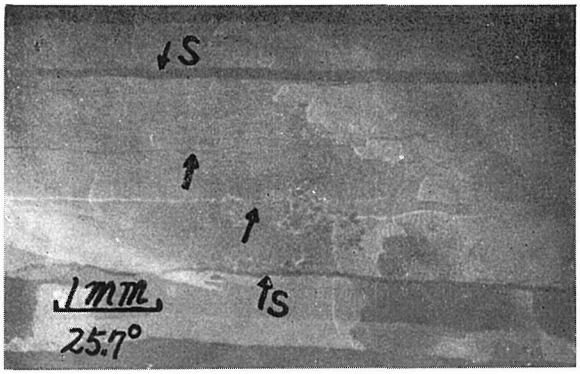


Fig. 11. X-ray micrograph of the side surface (001) of the specimen (99.99% pure tin) grown at 0.8 mm/min and 13°/cm. Fe K$\alpha$, reflecting plane : (332).

zone-refined tin shown in Fig. 4, were used as the material of the single crystal. The specimen was grown in the [110] direction at 0.05 mm/min. Fig. 12 shows the optical micrographs of the side surface (001) of the specimen mentioned above. (The left end of the lower photograph is near the seed.) The streaks vertical to the direction of growth are the banding structure[4].

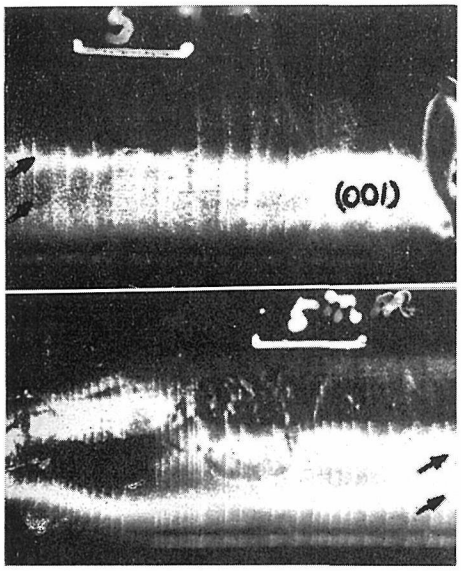


Fig. 12. Optical micrographs of the side surface (001) of the specimen (zone-refined tin) grown at 0.05 mm/min and 13°/cm. The left end of the lower photograph is near the seed.

Fig. 13 shows the Berg pattern of the specimen of Fig. 12. (The reflected image running obliquely in the top photograph is that of another plane.) The left of the bottom photograph is the image of the part near the seed, in which the substructures of irregular shape are observed. The differences in the crystallographic orientation could not be determined because of the low sensitivity

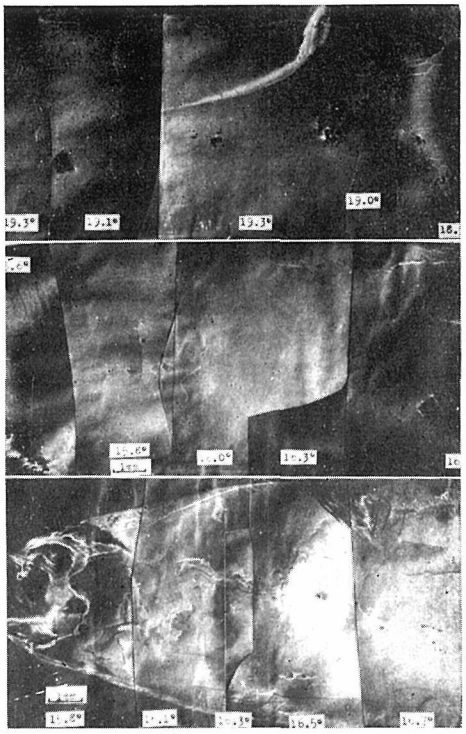

Fig. 13. X-ray micrograph of the specimen in Fig. 12. A series of reflected images taken by changing $\alpha$, were jointed together. Fe K$\alpha$, specimen face : (001), reflecting plane : (332).

of the equipment.*

The subboundaries of irregular shape are hardly observed in the central and top photographs, though they are clealy observed at the part which froze last (right end of the top photograph). As the specimen face-to-plate distance is largest at the right end of the photograph, the subboundaries can easily be detected. Therefore, the photographs were taken again by reversing the direction of specimen for the X-ray beam. The subboundaries, however, were still observed at this part.

As the concentration of solutes changes greatly at each streaks of the banding structure, the formation of substructures can be expected. However, it could not be confirmed in the present research.

## IV. DISCUSSION

Copper and lead were segregated at the part of the specimen which froze last as expected. Bismuth could not be purified well. When zone-refined at

* The specimen was slipped down on the desk carelessly. Therefore, the flaw and the strain are observed at the right upper part and at the left end of the bottom photograph respectively.

0.5 mm/min, however, it was rather segregated at the part of the specimen which froze late. Therefore, it is considered that the zone-refining should be performed at a very low speed.

Judging from the epuilibrium diagram, iron and antimony are expected to be segregated at the part which froze first. However, iron was always segregated at the part which froze last. Antimony was segregated at the part which froze first when its amount was relatively large, while it was segregated at the part which froze last when relatively small. The above result is unexplainable from the epuilibrium diagram of the tin-antimony system. Although these problems should have been investigated further, no sufficient examination on them was done because the study on the zone-refining was not the direct object of the present research.

As seen in Figs. 3 and 4, the amount of impurities is relatively large at the part which froze first. This would be attributed to the fact that only this part froze at a higher speed than that of the displacement of the electric furnace.

It was reported in Part I that the linear substructure developed more easily when the speed of growth and the temperature gradient were larger and that this substructure appeared more in number at the part which solidified later. In the present research too, the same result as reported in part I was obtained. (Figs. 5, 11 and 13).

The linear subboundary of a white or black line in the Berg pattern developed from the reticulate one of a white or black line respectively (Fig. 11). Therefore, a close correlation between these two substructures can be presumed.

When the speed of growth is large or when the dimensions of specimen change greatly, the uneven cooling is expected. Therefor, it is considered that the thermal stress caused by the uneven cooling becomes great and that the generation and movenment of dislocations are also great. The orientation difference of the subboundary developing from the seed changed greatly at the place where this intersected the reticulate subboundary of irregular shape (Fig. 6). Besides, a kind of fault was observed at the point on this subboundary. Therefore, it is considered that these reticulate subboundaries of irregular shape were formed after the solidification of the crystal.

In the specimen grown at 0.8 mm/min by using the zone-refined tin, some corrugations which developed discontinuously in the direction of growth were observed microscopically. In the X-ray micrograph, howevr, no linear substructure was observed (Fig. 10). The reticulate substructures of irregular shape were also fewer in number as compared with those in the specimen grown by using the raw tin (Fig. 5). Therefore, these discotinuous corrugations are cosidered not to have any relation to the development of linear subtructures.

No difference in the perfection of crystals was observed between two specimens which were grown at 0.8 and 0.05 mm/min respectively by using the zone-refined tin. Namely, at the speeds of growth within a certain limit, the speed seems to have no influence upon the perfection of crystals. Therefore, the necessary thing is high purity. As the reticulate substructures become fewer in number in the specimen grown by using the higher pure tin, the existence

of the dislocations, which are more in number than a certain limit, would be necessary for the formation of reticulate substructures.

The writer wishes to express his heartful gratitude to Prof. H. Takaki for his advice and encouragement in connection with this research, and to Dr. T. Sone and Dr. M. Kyōtani for their kindness with respect to the raw tin used in this research.

## REFERENCES

(1) W. G. Pfann *J. Metals*, **4**, 747 (1952).
(2) W. G. Pfann, *J. Metals*, **7**, 297, 961 (1955).
(3) M. Tanenbaum, A. J, Goss and W. G. Pfann, *J. Metals*, **6**, 762 (1954).
(4) M. Koxama, cf. reference (12) in Part I.
(5) A. J. Goss, K. E. Benson and W. G. Pfann, *Acta Met.*, **4**, 332 (1956).